Available online at www.sciencedirect.com

ScienceDirect

Energy Procedia 4 (2011) 3738–3745

Energy Procedia

www.elsevier.com/locate/procedia

GHGT-10

On the buffer capacity of CO_2-charged seawater used for carbonation and subsequent mineral sequestration

Domenik Wolff-Boenisch1*

Institute of Earth Sciences, University of Iceland, Sturlugata 7, 101 Reykjavik, Iceland

Abstract

Successful mineral trapping of carbon dioxide faces the challenge of effectively titrating a CO_2-charged acidic injection solution to pH conditions favorable to carbonate precipitation -using the rock as primary alkalinity source. To illustrate the magnitude of this task, buffer capacities of seawater solutions equilibrated with different partial pressure of CO_2 are presented, under open and closed conditions. A number of mechanisms can be evoked to overcome the large buffer intensity of the injection fluid, including dilution, dissolution kinetic catalysis and increasing reaction temperature. Buffer capacity – pH plots are presented to aid in understanding how buffer capacity changes as a function of the presence and concentration of key solutes, like fluoride.

Keywords: mineral sequestration; buffer capacity; titration; alkalinity; carbonation.

1. Introduction

Mineral sequestration is the fixation of CO_2 as stable carbonate minerals that provide a long-lasting, thermodynamically stable, and environmentally benign carbon storage solution. One option of CO_2 mineralization is injecting the gas after its dissolution into water into silicate rocks rich in divalent metal cations such as (ultra)mafic rocks [1]. The carbonation creates carbonic acid providing the protons required for rock dissolution and the release of divalent cations into solution. However, the mass of water required to fully dissolve one ton of CO_2 is large. At 25 bar pCO_2, 27 tons of pure water are required to dissolve a ton of CO_2. Likewise, the rock demand for mineral sequestration of carbon is huge. It takes at least 2.5 tons of basaltic glass to bind one ton of CO_2, assuming that the glass dissolves completely and that all divalent cations precipitate in carbonates [2]. To optimize this process, the fraction of liberated divalent cations that are eventually bound in carbonates versus other secondary minerals, such clays or zeolites, must be maximized.

Dissolved divalent metals can react with dissolved CO_2 to precipitate carbonate minerals according to:

$$M^{2+}(aq) + H_2O + CO_2(aq) \leftrightarrow MCO_3(s) + 2H^+ \quad (1)$$

This reaction illustrates the pH dependence of carbonate precipitation/dissolution. The reaction will proceed to the right only if the generated protons are consumed via host rock dissolution. However, field and experimental results suggest that the slowest and thus rate limiting step in mineral fixation of carbon in basaltic rock is the dissolution of silicate minerals and glasses. This study attempts to address the question whether sufficient alkalinity is generated by host rock dissolution to allow carbonate mineral precipitation. While reaction path models, for example PHREEQC [3], indicate silicate dissolution and carbonate precipitation will happen over time, such model calculations commonly assume batch conditions and do not take the continuous supply of carbonic acid to the system into account. This study

* Corresponding author. Tel.: +0-000-000-0000 ; fax: +0-000-000-0000 .
E-mail address: author@institute.xxx .

doi:10.1016/j.egypro.2011.02.307

presents the results of calculations aimed at quantifying the buffer capacity of various CO_2 charged waters and how they evolve in open and closed systems and in the presence/absence of specific solute ions.

2. Background

The buffer capacity ß (alternatively termed buffer index or intensity) describes the resistance of a solution to a pH change when either an acid or base are added (buffer solutions have therefore a large ß). Graphically, ß is the tangent line to any point on a titration curve (see Figure 1). The flatter the tangent line the smaller the amount of acid/base that has to be added to induce a change in pH and therefore the lower the buffer capacity. Conversely, a steep slope signifies that the solution has a high buffer capacity as the pH barely changes while base/acid is added. While the concept of buffer capacity has been treated extensively in (aquatic) chemistry textbooks [4, 5], its mathematical application and implication to fluid-rock interactions in carbon sequestration systems has not been explored. Of the few studies involving ß, [6] used the buffer capacity to describe the potential of basaltic rocks to buffer the pH of groundwater and [7] employed ß to define the 'proton driving force for reaction' in their studies on weathering phenomena in the Critical Zone.

ß can be described mathematically as the partial derivative of the change in alkalinity (A) with pH, either at constant pCO_2 or constant total carbon content C_T [8]:

$$ß\ (pCO_2, C_T) = d(A)/d\text{pH} \quad (2)$$

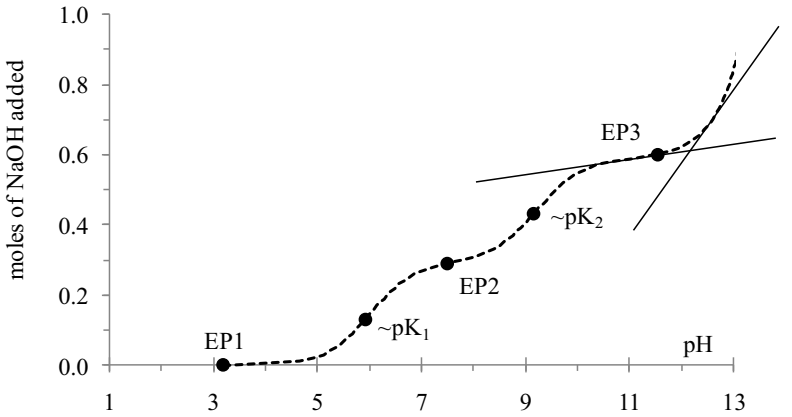

Figure 1 Titration curve for seawater that was equilibrated with a pCO_2 of 10 bar (initial pH 3.2) with equimolar steps of 1M NaOH. The slopes show the tangent lines at two different, but rather close alkaline pH. EP = equivalence point; for further explanation, see text.

Figure 1, which was generated with PHREEQC, also depicts five inflection points (3 equivalence points (EP) and 2 pK). EP1 represents the equivalence point of H_2CO_3* (H_2CO_3+CO_2, f=0), EP2 stands for the equivalence point of HCO_3^- (f=1), and the third EP corresponds to the equivalence point of CO_3^{2-} (f=2)[2]. Together with the two pK for the dissociation of carbonic acid these inflection points indicate that the tangent line at these specific pH go either through a maximum or minimum, respectively. This analysis can be used to determine if the system is well or poorly buffered. This is critical for CO_2 sequestration as it requires a combination of both, abundant protons to generate divalent cations from the silicate rock and a relatively unbuffered system that allows the fluid to evolve towards higher pH where these divalent cations can lock up carbon dioxide in carbonates.

3. Results and Discussion

Water availability is critical for CO_2 mineralization and may restrict its application in regions/countries with drinking water supply issues. In contrast, seawater is politically less sensitive and easier/cheaper to obtain when injection sites are close to or even in the ocean, such as sequestration in seafloor basalts [9]. Therefore it is essential to quantify the

[2] $f=(C_B-C_A)/C_T$ where C_B-C_A is the concentration of net strong base and C_T stands for the sum of individual carbon species

buffer capacity of injection solutions prior to and during their interaction with the host matrix. This study presents and discusses values of ß (eq/kg) that were calculated from total seawater alkalinity (2.3 meq/kg) at different concentrations of CO_2(aq). The total alkalinity TA can be defined as [10]:

$$TA = OH^- + HCO_3^- + 2CO_3^{2-} + B(OH)_4^- + H_3SiO_4^- + HPO_4^{2-} + 2PO_4^{3-} + HS^- + NH_3 - HF - HSO_4^- - H_3PO_4 - H^+ \quad (3)$$

Assuming a negligible effect of the phosphate and ammonia on seawater TA and re-writing Eqn. (3) with respect to pH and equilibrium constants at 25°C yields:

$$TA = \frac{K_w}{10^{-pH}} + \frac{C_T}{\frac{10^{-pH}}{K_{C1}} + \frac{K_{C2}}{10^{-pH}} + 1} + 2\frac{C_T}{\frac{10^{-2pH}}{K_{C1} \times K_{C2}} + \frac{10^{-pH}}{K_{C2}} + 1} + \frac{B_T \times K_B}{K_B + 10^{-pH}}$$

$$+ \frac{Si_T \times K_{Si}}{K_{Si} + 10^{-pH}} + \frac{S^*_T \times K_{S^*}}{K_{S^*} + 10^{-pH}} - \frac{10^{-pH} \times F_T}{K_F + 10^{-pH}} - \frac{10^{-pH} \times S_T}{K_S + 10^{-pH}} - 10^{-pH} \quad (4)$$

where K_{C1} and K_{C2} represent the first and second acidity constants of H_2CO_3*, and K_w, K_B, K_{Si}, K_{S*}, K_F, and K_S denote the equilibrium constants for the dissociation reactions of water, boric acid, silic acid, hydrogen sulphide, hydrofluoric acid, and bisulphate, respectively. C_T, B_T, Si_T, S^*_T, F_T, and S_T correspond to the total solute concentrations of carbon dioxide, boron, silica, sulphide, fluoride, and sulphate species, respectively. Sulphide concentrations are usually very low in seawater but have been kept in this calculation as redox processes may increase the sulphide content, enhancing alkalinity.

All equilibrium constants are expressed in terms of concentrations and were computed based on appendix A in [11] taking the effect of temperature, salinity, and ionic strength on the K values into account (Table 1). The minor effect of pressure on K values was ignored because a) it could not be retrieved for all relevant equilibrium constants in Table 1 and b) it was only found for the overall pressure and not partial CO_2 pressure. To calculate the partial derivative dTA/dpH of Eqn. (4) the following relationship is also required:

$$\frac{d}{dx}H^+ = \frac{d}{dx}10^{-pH} = -n \times 10^{-npH} \times LN(10) \quad (5)$$

Figure 2 summarizes the logarithms of ß calculated from Eqns. (4, 5) for three different initial CO_2 pressures. The five inflection points in Figure 1 correspond to three local minima (all EP) and two local maxima (both pK). It means that prior to reaction with the host rock the carbonated injection fluid is relatively unbuffered (EP1) and will, upon rock dissolution, rapidly increase in pH. Concomitantly, the buffer capacity rises proportionately, creating effectively a resistance to a further pH rise. Note, that with increasing initial pCO_2 EP1 shifts to lower pH and ß increases.

Table 1 Input parameters taken from [11] to calculate buffer capacities at standard conditions (25°C, 1bar, S=35, I=0.70 molal). The total concentrations of boron (B_T), fluoride (F_T), and sulphate (S_T) were calculated as a function of salinity [11], while those of silica (Si_T) and sulphide (S^*_T) were estimated.

pK_H	pK_w	pK_{C1}	pK_{C2}	pK_B	pK_{Si}	pK_{S^*}	pK_F	pK_S
1.547	13.217	5.847	8.966	8.597	9.384	6.510	2.518	0.999
				pB_T	pSi_T	pS^*_T	pF_T	pS_T
				3.381	5.180	6.000	4.155	1.549

This model is, however, only valid under circumstances where the total carbon content C_T remains constant, i.e., under closed conditions and in the absence of carbonate mineral precipitation. Such conditions may occur in zones of low permeability. However, close to the injection well and along preferential flow paths (via fracture flow), the system is certainly not closed as exchange of dissolved total carbon between fluid fractions of different reaction progress may occur. In such cases, calculations need to take account of changes in total dissolved carbon concentrations. The fundamental difference in the derivation of ß from closed versus open systems is that in the former case ß is calculated assuming a constant C_T while under open conditions, a constant pCO_2 is assumed. Thus, the second and third terms of Eqn. (4) which relate to the carbon species have to be replaced with:

$$TA = \cdots\cdots\cdots \frac{(pCO_2 \times K_{C1} \times K_H)}{\mathbf{10^{-pH}}} + \frac{2 \times pCO_2 \times K_{C1} \times K_{C2} \times K_H}{\mathbf{10^{-2pH}}} \cdots \quad (6)$$

where K_H stands for the Henry's constant of CO_2. The results of open system calculations are shown in Figure 3. ß derived from open system models exhibit V-shaped curves whose left sides correspond to the closed system curves. It is shortly after the first minimum that the open system curves increase monotonically without reaching a local maximum in their buffer capacity. This increase is due to the conversion of infinite amounts of $CO_{2(aq)}$ to HCO_3^- as the pH increases. At pK_1 (~5.9) ß from open system models are already 3.6 times higher than ß from corresponding closed system calculations. Extrapolating this difference to the second equivalence point (~7.4) would yield a 800fold increase in ß for the open system. This means that if injection and subsequent subsurface reactions were continuously taking place in an open system neutral pH would be very difficult to attain.

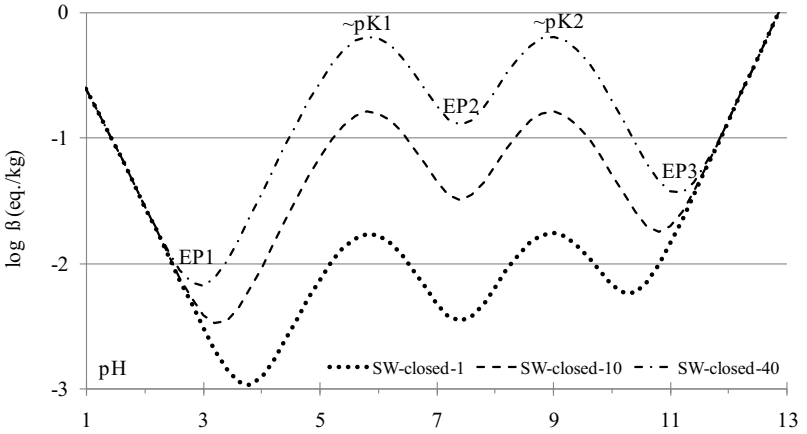

Figure 2 The buffer capacity ß of seawater (SW) as a function of pH for a *closed* system (C_T = constant). The three curves represent three initial pCO_2 (1, 10, 40 bar, from bottom to top) at carbonation. While they display the same shape their ß values vary in size because C_T is different in all cases.

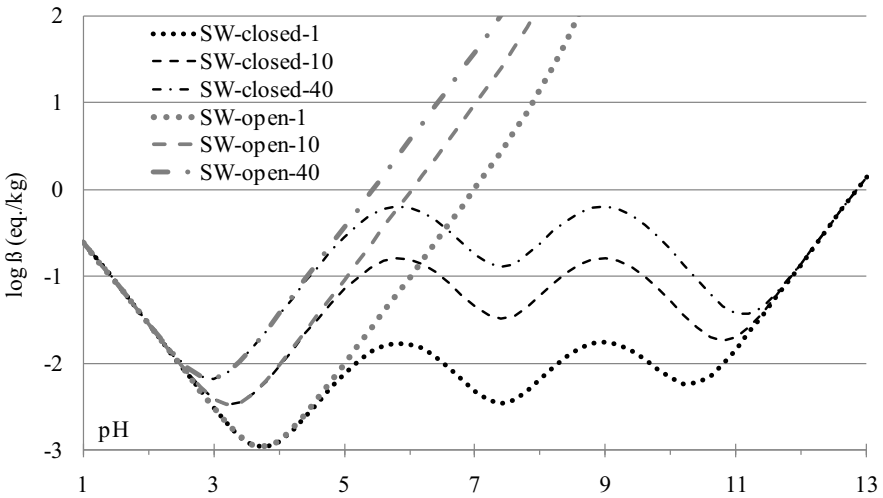

Figure 3 The buffer capacity ß of seawater as a function of pH for a closed (C_T = constant) and open system (pCO_2 = constant). The three wave-like curves are the same as in Figure 2 (i.e., closed system at 1, 10, and 40 bar pCO_2) while the three V-shaped curves represent open conditions during CO_2 mineralization: $C_T \neq$ constant and solution is in permanent equilibrium with a pCO_2 of 1, 10, and 40 bar, respectively.

These observations indicate that with increasing pCO_2 the buffer capacity of the injected solution could become a major hurdle for mineralization efforts. Titration of 1 kg of this acid solution at a pCO_2 of 40 bar with a strong base, such as NaOH, requires a staggering 500 mmol to reach a pH of 5.6 (for the closed system, modeled with PHREEQC).

Note, that an unbuffered solution would attain a pH of 13.5! This alkalinity is equivalent to that obtained from the dissolution of 150 g of MORB basalt provided that every proton is consumed by the dissolution reaction and based on a basalt molecular weight around 300 g/mol (cf. Table 1 in [12]). It is unlikely that, under the above mentioned injection conditions, per kilo of injection solution 150 g of basalt will dissolve to reach this pH. Thus, to attain a pH regime that can sustain carbonate precipitation additional processes need to occur, such as dilution of the injection fluid with the groundwater flow, enhanced dissolution kinetics of the host rock, and increase in temperature to reduce carbonate solubility. Figure 4 summarizes the crucial interplay between the key parameters total alkalinity (TA), dissolved inorganic carbon (DIC), and buffer capacity (ß). At the onset of injection, i.e., during carbonation, TA does not change. The dissolution of CO_2 into the fluid increases DIC which is limited by the solubility of CO_2 as a function of salinity, temperature, and pCO_2. This increase in DIC, however, does not affect TA because the acidity stems from the dissociation of carbonic acid creating equal amounts of protons and bicarbonate. Once the injected fluid starts dissolving the host rock (open circle) TA rises because protons are consumed and cations released. This reaction does not consume DIC but it changes the distribution of carbon species enhancing the amount of amphiprotic bicarbonate during this process. It is this amphiprotic character of bicarbonate that causes the rise in ß (illustrated by the open arrows in Figure 4) culminating in a local maximum at pK_{CI} which occurs roughly after a 300fold increase in TA, from 2.3 to 640 mmol/kg (300xSW in Figure 4, modeled with PHREEQC). The hatched lines stand for the solubility of magnesite (mag), calcite (cc), and siderite (sid), respectively. Titration and speciation calculations with PHREEQC under varying pCO_2 (=DIC) and incrementing pH (=TA) conditions yielded CO_3^{-2} solute concentrations that were compared to the respective solubility products of the above-mentioned carbonates, at 25°C (assuming metal concentrations equal to carbonate concentrations). Siderite is the least soluble carbonate of this comparison and requires relatively less alkalinity to reach saturation. This means that the pH does not have to go all the way against the buffer capacity to start (Fe)carbonate precipitation. However, as the slanted arrow indicates, carbonate precipitation reduces DIC by one and TA by two units, respectively. It is therefore not sufficient to reach saturation to *sustain* carbonatization, TA has to be replenished constantly.

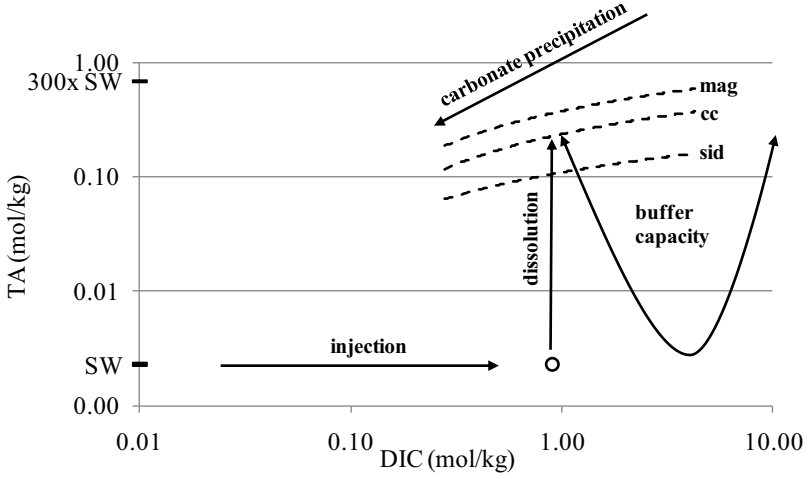

Figure 4 Relationship between total alkalinity (TA), dissolved inorganic carbon (DIC), and buffer capacity (ß) during the various stages of mineral sequestration: injection, dissolution, and precipitation. The open circle represents injection of carbonated seawater at 40 bar pCO_2. SW and 300x SW denote seawater alkalinity (2.3 mmol/kg), multiplied by 300 (690 mmol/kg). The buffer capacity increases with increasing TA during dissolution (open arrows). Mag, cc, and sid represent the solubilities at 25°C of magnesite, calcite, and siderite, respectively. See text for further explanation on TA and how the solubilities were calculated.

4. Conclusions

Calculating the buffer capacity ß of a CO_2(aq) system illustrates how much added alkalinity is required for injected CO_2 rich waters to attain carbonate mineral saturation and where the solution might be buffered against further pH changes. The linear increase of ß in Figs. 2 and 3 are such barriers. These barriers become tighter around the buffer minimum EP1 and will shift towards lower pH with increasing pCO_2. Hence, for carbonatization to occur, dilution of the initial pressurized fluid upon mixing with (alkaline) groundwater or added seawater may be required. Such a dilution and mixing with an alkaline fluid would diminish ß and raise TA. With increasing dispersion of the fluid away

from the injection well the system will become more closed creating a local buffer environment where carbonate precipitation can readily occur. Another option is the addition of specific ligands to the carbonation process that can accelerate dissolution kinetics of silicate minerals and glasses within the tight pH (2-5) envelope and thus produce alkalinity. However, dissolution as well as advection and dispersion are factors controlled by kinetics as well as hydrology and permeability that could change unfavorably in the reservoir over time. In contrast, enhancing temperature in the reservoir would decrease carbonate solubility and promote precipitation.

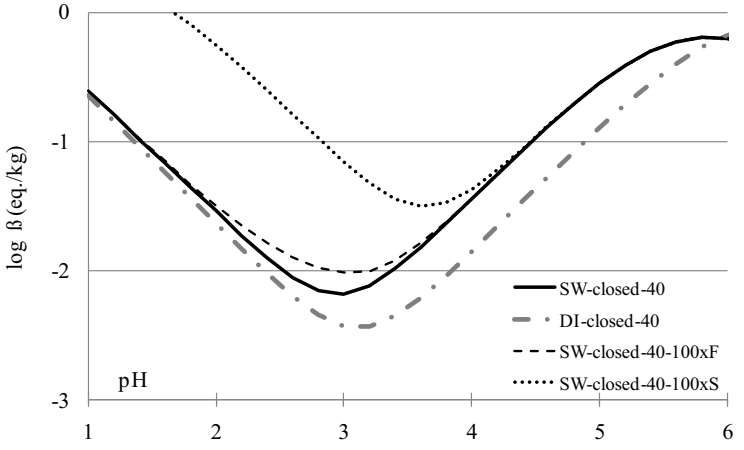

Figure 5 Buffer capacity versus pH of a seawater (SW) and pure water (DI) solution initially equilibrated with 40 bar pCO_2, under closed conditions. Different curves result when the seawater concentrations of fluoride and sulphate in table 1 (pF_T, pS_T) are multiplied by 100 (-100xF, -100xS).

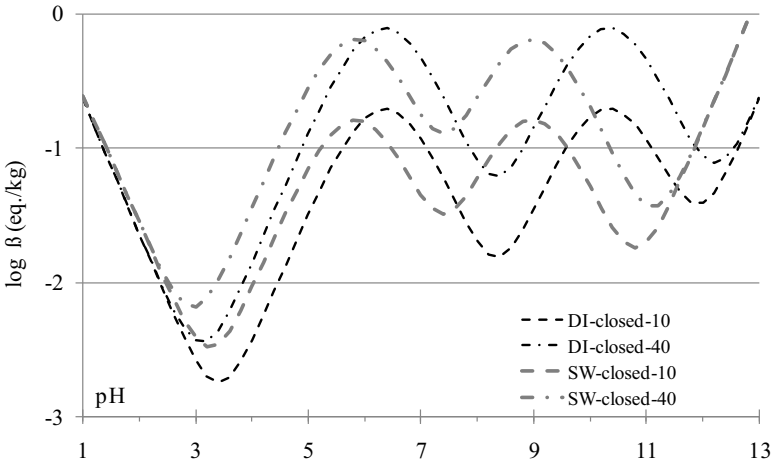

Figure 6 Buffer capacity versus pH of a pure water (DI) and seawater (SW) solution initially equilibrated with 10 and 40 bar CO_2, under closed conditions. DI-carbonated fluids have larger amplitudes resulting in larger ß values.

Creating ß vs. pH plots also illustrates how the buffer capacity changes as a function of the presence and concentration of key seawater ions, such as sulphate and fluoride, which promote dissolution rates of basaltic rocks [13, 14]. Figure 5 displays how the 40 bar pCO_2 curve from Figure 2 is altered in the presence of increased total sulphate (S_T) and fluoride (F_T) concentrations, respectively. Increasing the sulphate concentration of seawater (cf. pS_T in Table 1) by a factor of 100 (-100xS) moves the EP1 minimum towards higher pH but at the expense of an unwanted higher initial buffer capacity. In the case of increasing dissolved fluoride concentration (cf. pF_T in Table 1), however, a 100fold increase (-100xF) has only a marginal effect on ß. It has previously been shown that fluoride has a significant catalytic effect on volcanic rock dissolution [13] and so its negligible effect on ß makes it a prime choice as additive to the

injection solution. This example illustrates how this type of plot can be employed to modify the injection solution chemistry in a way that, by virtue of enhanced alkalinity generation, facilitates carbonate precipitation. The curve for de-ionized water (DI) has also been added to Figure 5 and Figure 6 to illustrate how ß changes for DI compared to seawater. All extrema of Figure 2 shift towards higher pH in desalinated solutions which is a result of consistently higher equilibrium constants (e.g., K_{c1}, K_{c2}, K_w) for low ionic strength solutions. Yet, the amplitude of these sinus curves increases in DI water meaning that relatively more mass of rock has to be dissolved to raise the pH compared to when seawater is the carbonation fluid.

5. Outlook

The presented calculations and conclusions are based on different geochemical models that are presumably not altogether consistent and therefore bear an inherent error. For example, ß was calculated without any computer code (just plain MS Excel™) while solubilities of CO_2 in seawater (DIC) at different pCO_2 were derived from [15, 16] and their respective webpage (http://www.geochem-model.org/models/co2-sea). Note that the variation in DIC between different models increases with increasing pCO_2 (Figure 7) and thus depend on the user's choice. Preference was given to the values obtained from the Duan group as they specifically address CO_2 solubilities in seawater. This DIC was subsequently introduced into PHREEQC, together with equilibrium constants and total concentrations extracted from [11] and compiled in Table 1 to calculate the evolution of TA and pH. Therefore caution must be exerted when introducing the presented data into reactive transport codes. Apart from the effect of ionic strength on the diverse parameters that make up this study, other caveats that may have affected the results are the ignorance of fugacity and redox processes. As to the former, only at 40 bar would it have been more appropriate to talk about fCO_2 instead of pCO_2 as the fugacity coefficient amounts to 0.8 [17]. With respect to the latter, fO_2 is certainly a parameter that has to be controlled and actually kept at a minimum but not so much because under reducing conditions sulphate could potentially be reduced to sulphide, thus increasing TA. Rather, oxidation of ferrous to ferric iron has to be avoided at all costs as this would diminish the potential of Fe-carbonate formation. The calculations presented above illustrate the need for fast and effective dissolution of the host rock to assure sufficient fluid neutralization for carbonate mineral precipitation. Mineral dissolution and precipitation reactions are generally proportional to the reactive surface area. Hence, in order to gauge the time required for neutralization, a good estimate of the reactive surface area is required which is highly speculative with respect to porosity, pore geometry, size and distribution, surface coatings and vesicle fillings, and ratio between glassy and crystalline portions of the basaltic reservoir. A comparable study found a 30-fold increase in alkalinity after injection of supercritical CO_2 into sandstone (Frio formation, Texas) in only three days [18]. However, this increased alkalinity as well as the rise in pH from an initially expected value around 3 to a measured one of 6 was not caused by *silicate*-fluid interactions. The authors ascribed the change in water chemistry to dissolution of calcite and Fe oxyhydroxides –contrary to the goals of mineral sequestration. Given that carbonate precipitation will eventually fill the rock pores, the key to increasing alkalinity lies in catalyzing the dissolution reactions in the reservoir rocks. In this regard, modification of the carbonation solution by addition of specific ligands appears to be a promising approach. Yet, more modeling and experimental work is required to refine the presented concept, factoring in time and homing in on an ideal carbonation solution for successful mineral trapping of carbon dioxide.

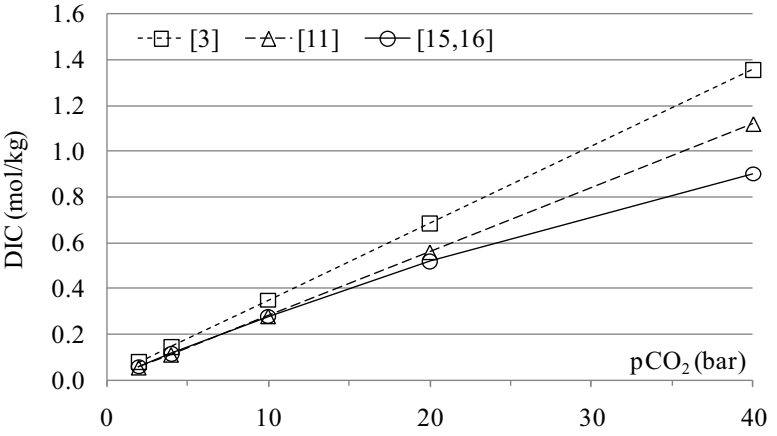

Figure 7 Variation in the determination of DIC from three different sources increases with increasing pCO_2. Numbers in brackets refer to the reference (25°C, S=35).

6. Acknowledgements

This study is part of the CarbFix project in Iceland (www.carbfix.com) and intellectual input from their members Sigurdur Gislason and Eric Oelkers is appreciated. Thanks go also to the Icelandic companies Reykjavik Energy, Nordurál, and Hitaveita Sudurnesja for their financial support.

7. References

[1] Gislason SR, Wolff-Boenisch D, Stefansson A, Oelkers EH, Gunnlaugsson E, Sigurdardottir F, et al. Mineral sequestration of carbon dioxide in basalt: A pre-injection overview of the Carbfix project. Int J Greenhouse Gas Control 2010; 4:537-545.
[2] Oelkers EH, Gislason SR, Matter J. Mineral carbonation of CO_2. Elements 2008; 4:333-7.
[3] Parkhurst DL, Appelo CAJ. User's Guide to PHREEQC (Version 2) -- A Computer Program for Speciation, Batch-Reaction, One-Dimensional Transport, and Inverse Geochemical Calculations. USGS Water Resources Inv Report # 99-4259.
[4] Morel FMM, Hering JG. Principles and Applications of Aquatic Chemistry. New York: Wiley-Interscience; 1993.
[5] Stumm W, Morgan JJ. Aquatic Chemistry, 3rd edition. New York: Wiley-Interscience; 1996.
[6] Gislason SR, Eugster HP. Meteoric water-basalt interactions. I: A laboratory study. Geochim Cosmochim Acta 1987; 51:2827-2840.
[7] Brantley SL, White AF. Approaches to Modelling Weathered Regolith. Rev Min Geochem 2009; 70:435-484.
[8] Butler JN. Ionic Equilibrium: Solubility and pH Calculations. New York: Wiley-Interscience; 1998.
[9] Goldberg DS, Takahasi T, Slagle AL. Carbon dioxide sequestration in deep-sea basalt. Proc Nat Acad Sci 2008; 105:9920-5.
[10] Dixon AG. An exact definition of total alkalinity and a procedure for the estimation of alkalinity and total inorganic carbon from titration data. Deep-Sea Res 1981; 28A:609-623.
[11] Zeebe RE, Wolf-Galdrow D. CO_2 in Seawater: Equilibrium, Kinetics, Isotopes. Amsterdam: Elsevier Oceanography Series 65; 2001.
[12] Wolff-Boenisch D, Gislason SR, Oelkers EH. The effect of crystallinity on dissolution rates and CO_2 consumption capacity of silicates. Geochim Cosmochim Acta 2006; 70:858-870.
[13] Wolff-Boenisch D, Gislason SR, Oelkers EH. The effect of fluoride on the dissolution rates of natural glasses at pH 4 and 25°C. Geochim Cosmochim Acta 2004; 68:4571-4582.
[14] Flaathen TK, Oelkers EH, Gislason SR. The effect of aqueous sulphate on basaltic glass dissolution rates. Min Mag 2008; 72:39-41.
[15] Duan ZH, Sun R. An improved model calculating CO_2 solubility in pure water and aqueous NaCl solutions from 273 to 533 K and from 0 to 2000 bar. Chem Geol 2003; 193:257-271.
[16] Duan ZH, Sun R, Zhu C, Chou IM. An improved model for the calculation of CO_2 solubility in aqueous solutions containing Na^+, K^+, Ca^{2+}, Mg^{2+}, Cl^-, and SO_4^{2-}. Mar Chem 2006; 98:131-9.
[17] Spycher N, Pruess K, Ennis-King J. CO_2-H_2O mixtures in the geological sequestration of CO_2. I. Assessment and calculation of mutual solubilities from 12 to 100°C and up to 600 bar. Geochim Cosmochim Acta 2003; 67:3015-3031.
[18] Kharaka YK, Cole DR, Thordsen JJ, Kakouros E, Nance HS. Gas-water-rock interactions in sedimentary basins: CO_2 sequestration in the Frio Formation, Texas, USA. J Geochem Explor 2006; 89:183-6.